IRANIAN JOURNAL OF CATALYSIS

Diisopropyl Ether Production via Isopropanol Catalytic Dehydration over Zirconium Phosphate Modified Natural Zeolite

Hasanudin Hasanudin[a,b,*], Wan Ryan Asri[a,b], Jeniva Rindi Anindia[a,b], Suheryanto Suheryanto[a,b], Zainal Fanani[a,b], Nino Rinaldi[c], Muhammad Al Muttaqii[c]

a) Department of Chemistry, Faculty of Mathematics and Natural Science, Universitas Sriwijaya, Indralaya 30662, Indonesia

b) Biofuel Research Group, Faculty of Mathematics and Natural Science, Universitas Sriwijaya, Indralaya 30662, Indonesia

c) Research Center for Chemistry, National Research and Innovation Agency(BRIN-Indonesia), Science and Technology Park B.J. Habibie, Serpong, South Tangerang 15314, Banten Indonesia

Received 13 August 2022; revised form 18 November 2022; accepted 12 December 2022 (**DOI: 10.30495/IJC.2022.1965421.1961**)

ABSTRACT

In this work, diisopropyl ether (DIPE) was produced through catalytic dehydration of isopropanol over zirconium phosphate-modified phosphate modified natural zeolite. The catalyst was prepared via the wet impregnation method. They were tested at 150 ˚C for 3 hours under a reflux system. The effect of zeolite-Zr$(H_2PO_4)_4$ metal loading and zeolite-Zr without phosphate incorporation on dehydration isopropanol was also assessed. The results showed the natural zeolite was successfully modified as confirmed by XRD, FTIR, SEM-EDX, N_2 physisorption, and catalyst acidity by the gravimetric technique. The highest isopropanol conversion (66.73%) was accomplished by 8 mEq/g zeolite-Zr$(H_2PO_4)_4$ followed by the DIPE yield and selectivity up to 35.81% and 47.8%, respectively. Further reusability investigation showed that zeolite-Zr$(H_2PO_4)_4$ catalyst provided adequate reusability up to the fourth reused with relatively decreased catalytic activity towards isopropanol dehydration.

***Keywords**: Diisopropyl ether, Iisopropanol Isopropanol conversion, Modification, Phosphate, Zeolite, Zirconium*

1. Introduction

Air pollution from gasoline fuel vehicles has become one of the most pressing issues in recent years, particularly in major cities [1]. Prolonged consumption of gasoline fuel, however, can potentially worsen the air quality. In this context, blending potential additive compounds into gasoline is one effective strategy to reduce air pollution. Besides, additives compounds are used to guarantee that fuels satisfy technical criteria or improve gasoline's performance and qualities [2]. Gasoline additives function as oxidizing agents, increasing octane number and combustion efficiency [3]. Until now, diisopropyl ether (DIPE) is the most critical oxygenated gasoline due to its eco-friendly chemical and anti-knocking properties [4]. DIPE can enhance the gasoline octane number in spark ignition (SI) engines and also has an appreciative vapor pressure of Reid mixture, abundant feedstock, and its solubility in water is only one-quarter of MTBE [5]. Kale et al. [6] reported that the NO_x emission on HCCI combustion could reduce from 96 ppm to 81 ppm as the increase of DIPE load from 10 to 60% on gasoline blends. Uyumaz et al. [7] reported that the DIPE with 40% loaded could increase the power output to 24.7% at a lambda of 2 and 1000 rpm with a maximum indicated thermal efficiency of 23.4% at a lambda of 2.33 on HCCI combustion, which suggested that DIPE may be able to increase the range at which HCCI can operate while preventing knocking. Further, diisopropyl ether is regarded as a cost-effective and eco-friendly fuel additive based on its effect on the heat release rate and cylinder pressure study on HCCI combustion.

At this time, the production of DIPE has widely been substantially conducted through a typical dehydration reaction of alcohol-based feed stocks with various acidic

*Corresponding author:
E-mail address: hasanudin@mipa.unsri.ac.id (**H. Hasanudin**)

catalysts and conditions reactions. It is well known that the catalyst's performance is strongly correlated to the efficiency of DIPE production, consequently, the development of a suitable catalyst currently has considerable attention. A typical of oxide-based such as Al_2O_3, SnO_2, TiO_2, Fe_2O_3, ZrO_2, SnO, MgO, MoO_3 [8,9], Al_2O_3–TiO_2 [10], ZrO_2-SiO_2 [11], semicrystalline polyethylene-grafted sulfonated styrene [12], supported iron oxides [13], keggin-type heteropolyacids supported ZrO_2 [14], Ni-W Sulfides [15], ion exchange resin [16], zeolite-based catalysts and their modifications [3,17], have been extensively proposed as dehydration reaction's catalyst. These catalysts exhibited high conversion at certain conditions. However, some of these catalysts have drawbacks due to low selectivity and yield towards DIPE and require high-cost precursors. Particularly, typical alumina-silicates such as modified zeolite-based catalysts catalyst quite fascinating due to their acidic nature, which provides both Brønsted and Lewis acid sites and porous so that promote the dehydration of alcohol-involved reactions as well as many typical reactions [18–22]. Zeolite has high stability and adjustable acid porosity and texture properties, so it is broadly employed as an environmentally friendly support catalyst [23]. Several catalysts such as Ni-W modified ZSM-5 and β-zeolite [17], Ni–Cu–Cr/H-Zeolite-β [3], have been utilized for dehydration reactions. At the present, transition metal phosphate materials such as zirconium phosphate are increasingly enchanted research interest due to their exceptional physical and chemical features, including a prominently high ion-exchange capability and magnificent thermal stability. Because of these outstanding characteristics, as well as their ease of synthesis and functionalization, zirconium phosphate materials are intriguing prospects for a wide range of applications [24–28]. Zirconium phosphate can be easily assembled by functional groups due to the presence of a moderately strong brønsted P-OH group [29,30], which has the potential to catalyze alcohol dehydration reactions. Zirconium involving zeolites is recognized for its excellent stability and easy regeneration by calcination [31]. They have a broad implementation of catalytic reactions, especially in reactions requiring desired acidity and oxidizing ability [32]. The modification of zeolite using zirconium phosphate can potentially promote the catalytic activity towards isopropanol to diisopropyl ether through a positive effect of alternative high acidic sites of both materials with synergetic textural properties.

In regards to economical cost and complex preparation concerns, the enlargement of low-cost catalysts has been pointed to utilizing natural zeolite due primarily to their abundant presence and cost-effectiveness compared with synthetic zeolite [33]. To the best of existing knowledge, neither studies nor reports have been yet revealed regarding the modification of natural zeolite using zirconium phosphate for isopropanol conversion to DIPE via dehydration reaction. In this research, the zirconium phosphate-zeolite and its catalytic activity will be compared with the zirconium uncontained phosphate-zeolite.

2. Experimental

2.1 Preparation of zeolite

Initially, 200-mesh natural zeolite (Bayan, Central Java) was dried in an oven at 393.15 K for 3 hours and then cooled in a desiccator. Afterward, 100 g of natural zeolite was immersed in a hydrogen fluoride solution (1 %), subsequently stirred for 1 hour, and then washed with distilled water 7 times each for 24 h. The natural zeolite was later immersed in a 6 N HCl solution (125 mL) for 4 hours, separated, and rinsed with DW until the pH was nearly neutral [34].

2.2 Synthesis of zeolite-$Zr(H_2PO_4)_4$

Zeolite-$Zr(H_2PO_4)_4$ was synthesized using the impregnation method with $ZrOCl_2.8H_2O$ (≥ 99% purity, Merck) as a Zr^{4+} precursor. Firstly, 5 g of as-prepared natural zeolite was dispersed on 0.1 M $ZrOCl_2.8H_2O$ solution by varying the volume of Zr^{4+} precursor (25, 50, 70, 75, 100, and 125 mL corresponding to 2, 4, 6, 8, 10 mEq/g, respectively) and stirred for 1 hour utilizing a magnetic stirrer (SH-2 Corona) at an ambient temperature. Afterward, the 1 M $NH_4H_2PO_4$ (≥ 99% purity, Merck) solution was gradually dropped using a burette into the mixture at a rate of 1 mL/min until it reached 10, 20, 30, 40, and 50 mL volumes, corresponding to 2, 4, 6, 7, 10 mEq/g of zirconium phosphate, respectively, and stirred for one day. After impregnating process, the temperature was increased by 353.15 K until the solution formed a paste. The paste was later washed with distilled water until free from Cl^- ions. The free Cl^- ions can be indicated by no white precipitation on the filtrate formed after being tested by the $AgNO_3$ solution (0.01 M). The paste was dried in an oven at 378.15 K for 24 h. The solids were then crushed and sieved through a 200-mesh sieve and then calcined at 623.15 K for 4 hours. The zeolite-Zr was synthesized as the same as zeolite-$Zr(H_2PO_4)_4$ as previously described, but without involving $NH_4H_2PO_4$ solution.

2.3 Catalyst characterization

The crystal structure and phase of natural and modified zeolite were assessed using the X-ray diffractometer

Rigaku MiniFlex 600 (Japan). FTIR Shimadzu-Prestige 21 (Japan) was utilized with the KBr pellet technique for functional group analysis (recorded from 4500 to 500 cm^{-1}). The textural characteristic was evaluated using N_2 physisorption at 77.35 K in a Quantachrome instrument (USA). The catalyst was vacuum degassed to 300 ˚C with a heating rate of 10 ˚C/min for 60 min. The multi-point BET method was employed to determine the catalysts' surface area, the pore features were determined by the BJH method, whereas the external surface area and the micropore area were evaluated using the t-plot method. The catalysts' morphology and elemental composition were inspected using a Tescan Vega 3 (Czech Republic) scanning electron microscope (recorded at 5000× magnification with HV of 15 kV) assisted with X-ray energy dispersive spectroscopy (Bruker QUANTAX, US). The gravimetric method was employed to evaluate the surface acidity features of catalysts utilizing a pyridine base [35].

2.4 Dehydration of isopropanol

The activities of the catalysts were evaluated by the dehydration of isopropanol, performed in a batch reactor consisting of a reflux system (graham condenser) and a 3-neck round flask (100 mL) as a sample container. The round flask was placed in an oil bath equipped with a thermometer, and the temperature of the reaction was controlled by the hot plate (**Fig. 1**) using 50 mL of isopropanol and 0.5 g of catalyst. The conversion of isopropanol to the diisopropyl ether was conducted at 423.15 K for 3.5 h. After execution of the reaction, the catalyst was separated with the solution and washed with acetone followed and dried at 120 ˚C for 12 hours and utilized for the next cycle.

Reaction products were determined using GC-MS (Thermo Fisher Scientific) with TG-5MS columns. The initial oven programmed temperature was 32 ˚C for 2.5 min and ramped at 3˚C/min to a final temperature of 45 ˚C for 2 min, with a He as a carrier gas (1 mL/min). The injection temperature was 200 ˚C. The MS transfer line temperature was 230 ˚C, whereas the ion source temperature was 210 ˚C. The reaction characteristics were described as follows:

$$IPA_C = \frac{\alpha_0 - \alpha}{\alpha_0} \times 100 \quad (1)$$

$$DIPE_Y = \frac{\beta \times 2}{\alpha_0 - \alpha} \times 100 \quad (2)$$

$$DIPE_S = \frac{\beta}{\alpha_0} \times 100 \quad (3)$$

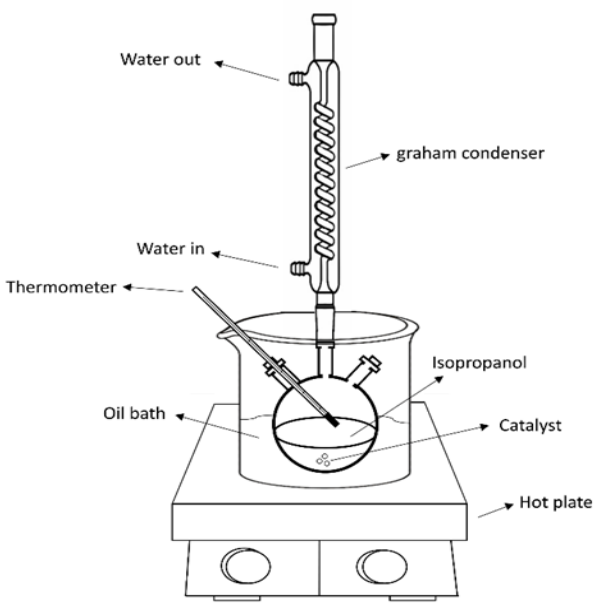

Fig. 1. Schematic diagram of dehydration reaction

Where α_0 and α are denoted as isopropanol initial and final moles, respectively, whereas β is denoted as diisopropyl ether product mole. IPA_c, $DIPE_Y$, and $DIPE_s$ are denoted as isopropanol conversion, DIPE yield, and selectivity, respectively.

3. Results and Discussion

3.1 Characterization of natural and modified zeolite

Natural and modified zeolites were assessed using various characterizations. **Fig. 2** depicts the diffractograms of all catalysts. It appeared that the natural zeolite had three major constituents, which consisted of mordenite, clinoptilolite, and quartz. A comparable result was also outlined consistently by previous works when assembling unmodified zeolite, which revealed that the natural zeolite existed in many phases [36–39]. The diffraction peaks at 2θ of 22.26˚, 25.61˚, and 27.56˚ were attributed to the mordenite phase (JCPDS No. 6-239) [40], whereas the clinoptilolite phase was identified at 2θ of 9.75˚, 13.45˚, and 29.77˚ (JCPDS No. 17-0143) [33]. Another quartz phase was also noticed at 2θ of 19.61˚ and 26.16˚ (JCPDS 46-1045). Abreu et al. [41] reported that typical natural zeolite had the highest composition of minerals of mordenite, followed by clinoptilolite and quartz with the lowest composition.

As can be discerned in **Fig. 2**, no appreciable new phase formed on the modified zeolite, which suggested that zirconium, as well as zirconium phosphate, were finely dispersed on the natural zeolites by assembling small Zr

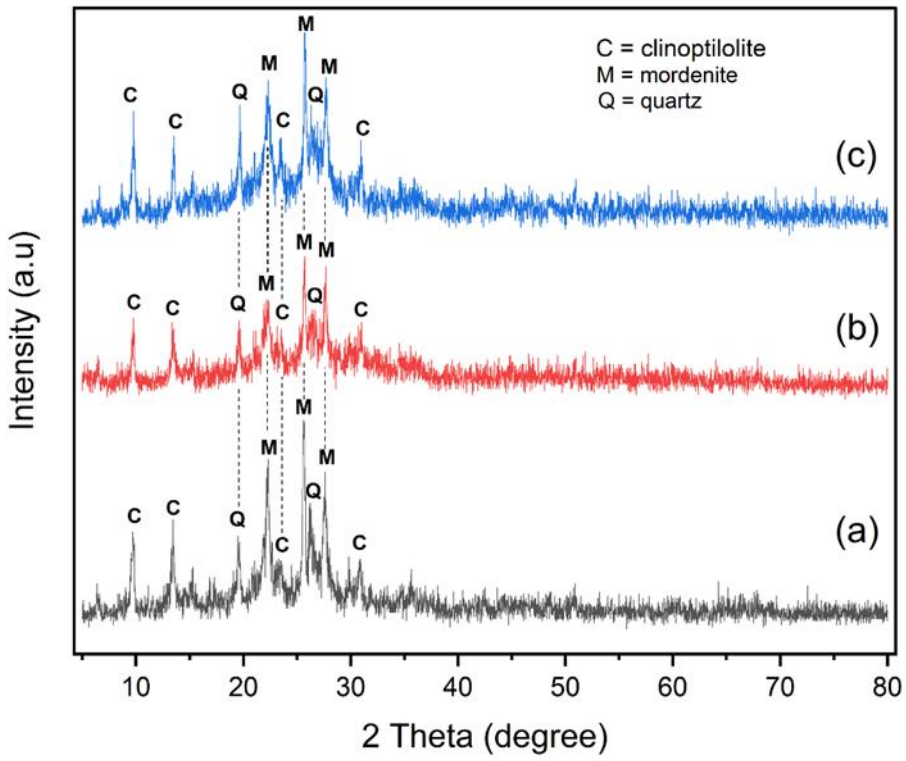

Fig. 2 XRD spectra of (a) NZ (b) NZ-Zr (c) NZ-Zr$(H_2PO_4)_4$

and Zr$(H_2PO_4)_4$ species that were under observation limit of XRD quantification [42]. Ma et al. [43] observed that there were no distinctive peaks of Y-zeolite and zirconium-modified Y-zeolite, which attributed to no transformation of crystal form. The typical phase of natural zeolite still existed after modification, indicating that the framework structure of natural zeolite was not altered after incorporating Zr heteroatoms into the natural zeolite [44]. Furthermore, there were slight shifts of 2θ from ~20 to 30˚ after natural zeolite modification using zirconium and zirconium phosphate, which was presumably due to the stress formation by the dissimilarity in ionic size between natural zeolite, Zr, and Zr$(H_2PO_4)_4$ ions [45]. The vanishing or suppression relative intensity of natural zeolite after modification was also observed in **Fig. 2** as studied by Valdés et al. [46] on the Cu/zeolite.

The micrographs of both zeolite and their modification recorded by SEM are presented in **Fig. 3**. As shown in **Fig. 3a**, zeolite had irregular surface morphology with different thicknesses, with a platy sheet-like structure. These typical natural zeolite structures were also reported by other studies [39,47]. Mehdi et al. [48] reported that natural zeolite, which consisted of mordenite minerals, had a bumpy and rough surface, whereas the clinoptilolite mineral of natural zeolite had a typical platelet-like structure [45]. Mansouri et al. [49] also reported that lamellar texture zeolite typically existed on zeolite containing clinoptilolite minerals. Based on **Fig. 3**, it can be seen that the morphological surface of natural zeolite was distinctly more uneven and had a slight bulge after being modified, which presumably arose from zirconium and zirconium phosphate species, respectively. Similarly, Ma et al. [43] showed that there were tiny lumps and uneven structures existed after the modification of zeolite using zirconium. In particular, the zeolite-Zr$(H_2PO_4)_4$ morphological surface had a relatively irregular bulky structure compared with zeolite-Zr, which suggested that instinctive active site, i.e., zirconium phosphate, was dominantly presented in the zeolite framework. This assumption was corroborated by Domenzain-Gonzalez et al. [50] who stated that irregular structure could promote a greater active site.

The elemental composition of catalysts evaluated using EDX instrument is demonstrated in **Table 1**. It appeared that Si (37.75%), Al (5.78%), O (50.64%), and impurities (6.53%) were the primer constituent element in the natural zeolite. These impurities consisted of alkali and alkali metals and also some transition metals which typically existed on as-prepared natural zeolite [51,52]. A new constituent element of Zr (3.09%) on zeolite-Zr, also Zr (3.1%) and P (1.23%) on zeolite-Zr $(H_2PO_4)_4$ were present after natural zeolite modification, indicating that the modification of natural zeolite through impregnation method was favorably achieved.

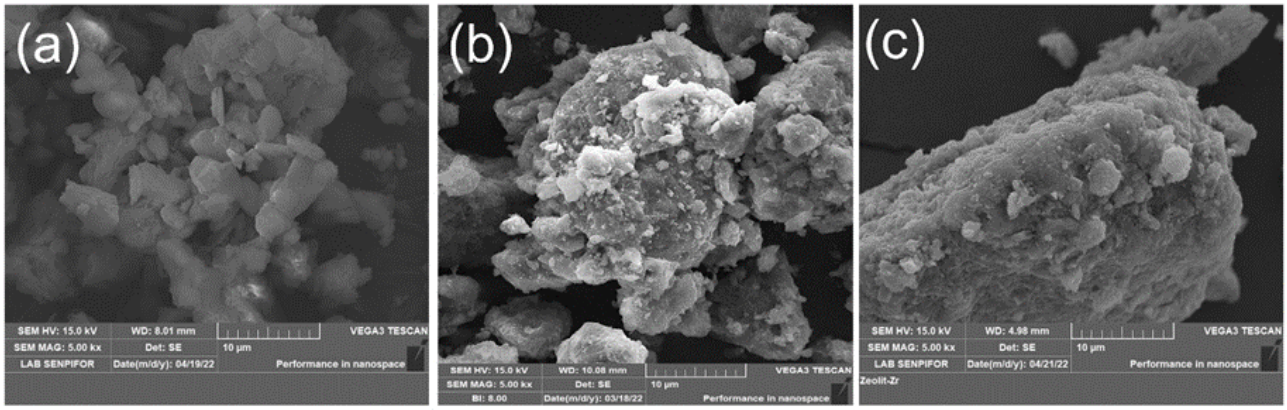

Fig. 3 SEM images of (a) NZ (b) NZ-Zr (c) NZ-Zr$(H_2PO_4)_4$

Table 1. Elemental analyses of catalyst by EDX

Elements	Atomic (%)		
	NZ	NZ-Zr	NZ-Zr$(H_2PO_4)_4$
Si	37.75	32.72	22.28
Al	5.78	5.02	3.48
O	50.64	53.92	64.37
Zr	-	3.09	3.1
P	-	-	1.23
Impurities	5.83	5.25	5.54
Si/Al	6.53	6.52	6.4

Permata et al. [53] also reported a similar finding when modifying the natural zeolite using Ni, which revealed that the presence of Ni after zeolite modification, analyzed by EDX, suggested the positive results of the impregnation method. Furthermore, the Si/Al ratio of natural zeolite and modified zeolite were relatively constant, which suggested that the s natural zeolite structure was maintained during the impregnation [54,55]. This SEM-EDX result was consistent with the XRD analysis results.

The N_2 physisorption of zeolite and modified zeolite were presented in **Fig. 4**. As can be seen that the N_2 adsorption-desorption of natural zeolite and modified zeolite were relatively the same, demonstrating that the zeolite structure was not changed by Zr and Zr$(H_2PO_4)_4$ impregnation. This situation was also described by Alalga et al. [56] which revealed that the N_2 physisorption of parent zeolite was relatively unchanged after Ni impregnation. Based on IUPAC categorization, the N_2 physisorption in **Fig. 4** revealed type IV isotherms with H4 type hysteresis loop. This type IV corresponded to mesoporous as well as microporous catalysts [56,57], whereas The H4 type was attributed to the narrow slit-like pores generated by plate-like species aggregation [32]. Furthermore, at relative pressure 0.4-0.7, N_2 adsorption-desorption of zeolite-Zr$(H_2PO_4)_4$ and zeolite-Zr had a likely change of hysteresis loop compared with natural zeolite, presumably due to the presence of mesoporous as well as microporous structure generated on the zeolite surface by Zr and Zr$(H_2PO_4)_4$.

The textural features of catalysts are demonstrated in **Table 2**. The natural zeolite had 137.26 m^2/g surface area and decreased to 133.75 m^2/g and 111.21 m^2/g after the modification of Zr and Zr$(H_2PO_4)_4$, respectively, as well as decreased the micropore area. This decreased surface area was presumably due to blocking pores with Zr and Zr$(H_2PO_4)_4$ species, particularly located at micropore areas [55,58]. This circumstance was also described by other works regarding decreased natural zeolite surface area after modification [53,59–61]. Meanwhile, the increase in the external surface area of natural zeolite was presumably due to the distribution of Zr and zeolite-Zr$(H_2PO_4)_4$ species which expand the pore on the surface of zeolite [62]. The decrease in average pore size and total pore volume after modification, justified the successful incorporation of Zr and Zr$(H_2PO_4)_4$ on zeolite pores [63].

The FTIR spectra of natural zeolite and modified zeolite are presented in **Fig 5**. The band at 3466 cm^{-1} corresponded to the Si/Al-OH or metal-OH tensile vibration on the surface of the framework natural zeolite [64]. The SiO_4 or AlO_4 vibrations were observed at the

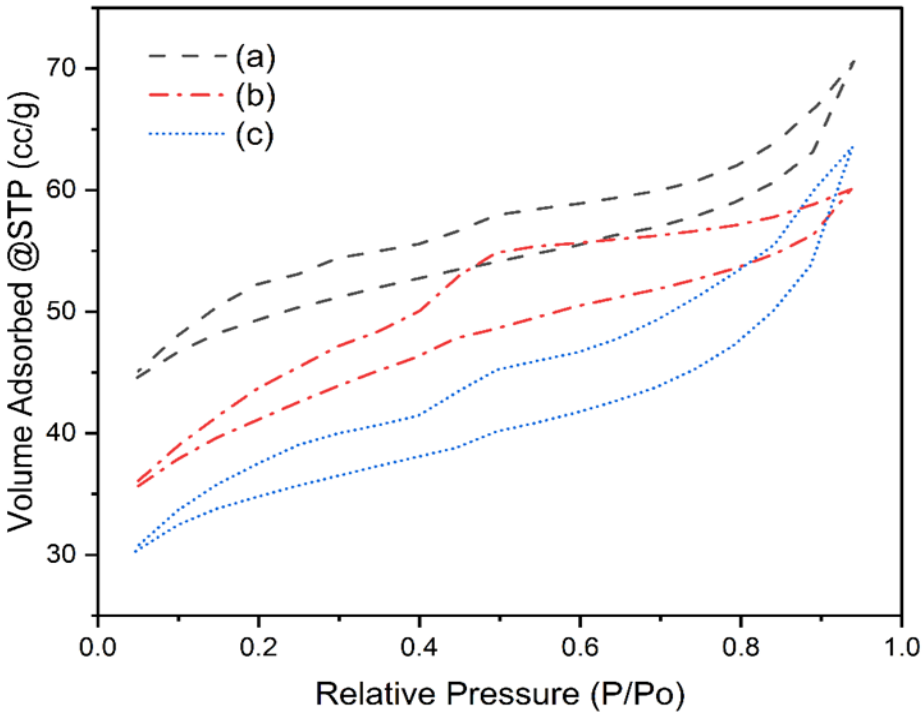

Fig. 4 N_2 physisorption of (a) NZ(b) NZ-Zr and (c) NZ-Zr$(H_2PO_4)_4$

Table 2. Textural features of catalysts

Catalyst	S_{BET} (m^2/g)	$S_{external}$ (m^2/g)	Micropore area (m^2/g)	Total pore volume (cm^3/g)	Average pore size (nm)
Natural zeolite	137.26	34.05	103.21	0.11	1.42
Zeolite-Zr	133.75	55.48	78.27	0.09	1.39
Zeolite-Zr$(H_2PO_4)_4$	111.21	38.31	72.89	0.08	1.27

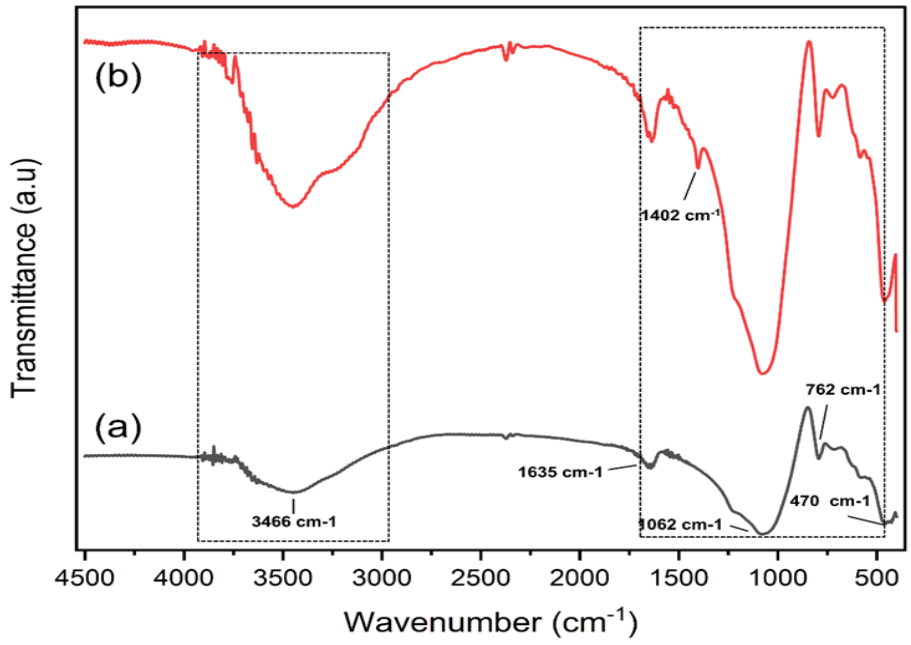

Fig. 5 FTIR spectra of (a) zeolite-Zr and (b) zeolite-Zr$(H_2PO_4)_4$

1062 cm^{-1} band [48]. The band at 1635 cm^{-1} corresponded to the O-H deformation vibration from the H_2O molecule [44], whereas the bending vibration of Al-O and Si–O was noticed at the 762 cm^{-1} bands [65]. The Zr-O stretching vibration was observed at 470 cm^{-1} [28,66,67]. Those bands were presented in both zeolite-Ni and Zeolite-Zr$(H_2PO_4)_4$ catalysts. The new bands were observed at 1402 cm^{-1} which ascribed to the P-O-Zr vibration [68]. Some studies reported that the vibration of PO_4^{3-}, P-O, and P-OH groups were observed at 1000-1200 cm^{-1} [28,69–71], which likely overlapped over both modified zeolites. However, there was a significantly increased intensity at certain bands on the zeolite-Zr $(H_2PO_4)_4$ FTIR spectrum, which indicated presumably due to the effect of the presence of phosphate ions as well as the interaction between the zeolite framework and zirconium phosphate species. The FTIR investigation corroborated the fabricated of the modified zeolite.

The acidity of zeolite-Zr and zeolite-Zr $(H_2PO_4)_4$ measured utilizing the gravimetric method is presented in **Fig. 6**. The zeolite-Zr catalyst had a low acidity value of 0.7245 mmol pyridine/g catalysts, which came from a low acidic site of alumina-silicate obtained from zeolite [19] as well as zirconium oxide [72]. The zeolite-Zr$(H_2PO_4)_4$ at 2 mEq/g metal loading had an acidity of 0.7358 mmol pyridine/g catalysts, which was higher than a zeolite-Zr catalyst, which suggested that the phosphate species (P-OH) provided an alternative brønsted acid site, which contributed to the increased catalyst acidity [73,74]. This condition was also justified by Palomo et al. [75], which stated that the increase in the catalyst's acidity was closely related to the existence of Zr-O-P species, which behaved as the acid site of the catalyst. Moreover, the acidity of the catalyst was increased up to 2.49% when the metal loading was 4 mEq/g which generated catalyst acidity of 0.7541 mmol pyridine/g catalysts. Furthermore, prolonged metal loading increased the catalyst's acidity due to a more acidic site [76]. As shown in **Fig. 6**, the highest catalyst acidity was accomplished by 8 mEq/g metal loading with the acidity of 0.8816 mmol pyridine/g catalysts. Furthermore, there was an appreciable decrease of catalyst acidity to 0.8514 mmol pyridine/g catalyst at metal loading, presumably due to agglomeration that could obstruct the acidic site of the catalyst directing to a decrease in the catalyst's acidity [77,78]. This condition was also consistently reported in by the previous study [20]. Based on these results, the zirconium phosphate species could enhance the acidity, which instinctively affects the catalytic activity toward alcohol dehydration reaction.

3.2 Catalytic activity towards isopropanol dehydration

The activities of zeolite-Zr and zeolite-Zr$(H_2PO_4)_4$ with various metal loading were utilized for the dehydration of isopropanol under the same conditions. The catalytic activity features of isopropanol conversion, DIPE yield, and selectivity are presented in **Fig. 7**. As revealed in **Fig. 7**, zeolite-Ni was moderately active, which generated 44.7% towards isopropanol conversion. The isopropanol conversion was improved up to 50.81% when employing the catalyst of zeolite-Zr$(H_2PO_4)_4$ at 2 mEq/g metal loading. This situation suggested that the zirconium phosphate positively affected the isopropanol conversion, which could be explained by on the phosphate interaction with the zirconium which promoted more acidic site and was responsible for the dehydration of isopropanol. Furthermore, prolonged metal loading generated higher isopropanol conversion but tended to decrease when the metal loading was 10 mEq/g (59.75 %). This trend was similar to catalyst acidity properties, which implied that the conversion of isopropanol was positively correlated to the acidity of the catalyst. A similar trend reported by the previous study was also coherent with the results of this study [20]. The highest isopropanol conversion (66.73 %) was accomplished by zeolite-Zr$(H_2PO_4)_4$ 8 mEq/g catalyst loading. Yaripour et al. [79] observed that the catalytic activity of γ-Al_2O_3 was remarkably enhanced after being modified with phosphorous to a certain extent.

The effect of zeolite-Zr and zeolite-Zr$(H_2PO_4)_4$ with various metal loading on the DIPE yield and selectivity are depicted in **Fig. 7**. It can be noticed that zeolite-Zr produced 20.38% of DIPE yield with only DIPE selectivity of 4.19%. At low metal loading of zeolite-Zr$(H_2PO_4)_4$, the DIPE yield increased up to 24.32%, and the DIPE selectivity was also risen significantly up to 32.49%. This condition justified that the modified zirconium phosphate catalyst also affected the DIPE yield and selectivity. Said and El-Aal [80] stated that the catalytic activity towards alcohol dehydration greatly depends on the metal's properties and the metal loading. As revealed in **Fig. 7**, a prolonged metal loading also increased the catalytic activity towards DIPE yield and selectivity with no further significant increase at high metal loading (10 mEq/g). A similar condition was also described by Palomo et al. [75] who observed high catalyst loading likely generated relatively constant results towards methanol conversion and dimethyl ether selectivity. Based on these outcomes, it concluded that a metal loading of 8 mEq/g could be examined as the optimum condition that generated the highest DIPE yield and selectivity of 47.85% and 35.82%, respectively. Ni et al. [81] reported that the performance

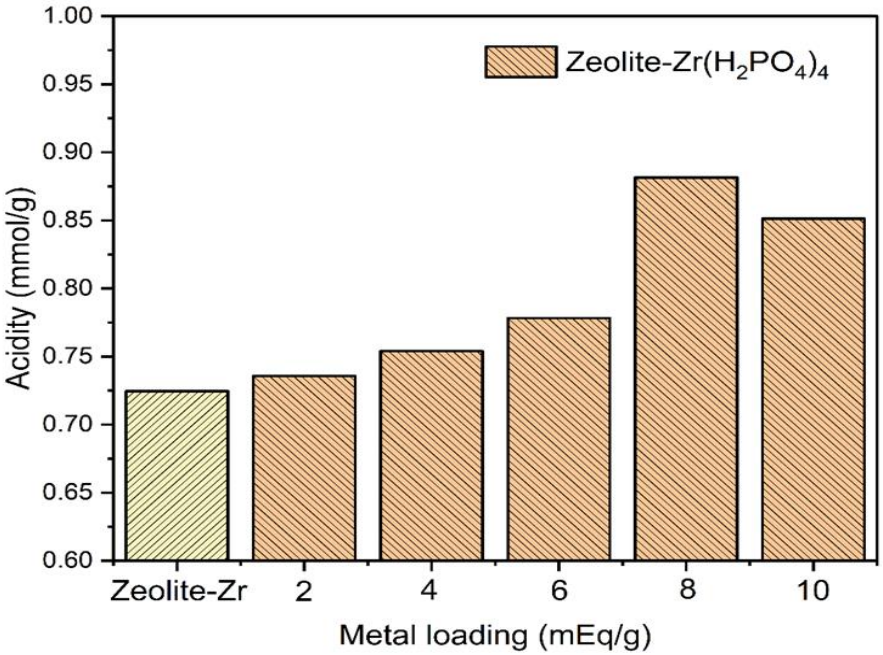

Fig. 6 Acidity of zeolite-Zr and zeolite-Zr$(H_2PO_4)_4$ with various metal loading

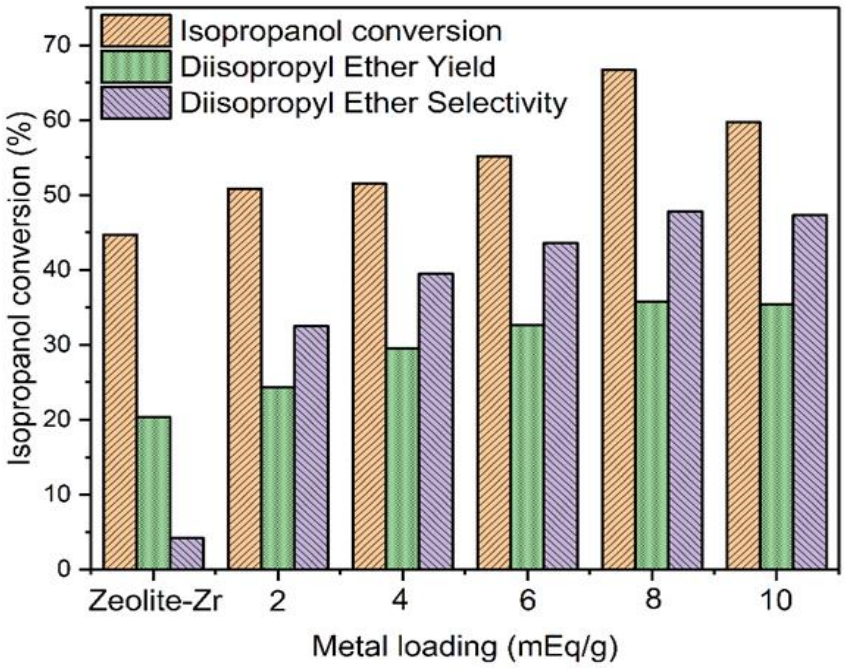

Fig. 7 The isopropanol conversion, DIPE yield, and selectivity catalyzed by zeolite-Zr and zeolite-Zr$(H_2PO_4)_4$ at various metal loading

of the dehydration reaction was dependently related to the acidity of the catalyst, in which more acid sites could intensify the catalytic activity. Moreover, some studies study reported that the decrease of surface area could promote promotes the selectivity towards DIPE [82], and this condition was likely consistent with the textural features of the catalyst, which showed that zeolite-Zr$(H_2PO_4)_4$ exhibited a higher reduction of zeolite surface area compared with zeolite-Zr. Besides, the pores generated by zeolite-Zr$(H_2PO_4)_4$ through the impregnation method presumably expand accessibility to acid sites and promotes the reactants and products diffusion rate [83], as a consequence, higher the selectivity and yield toward DIPE. The production of DIPE through isopropanol dehydration required two molecules of isopropanol which were subsequently absorbed in the Lewis and Bronsted acid site's active site [8]. The hydroxyl group attached to the acid center and

produced a carbocation reacted with the nucleophilic through substitution reaction and finally generated a DIPE product followed by deprotonation. The previous study regarding the dehydration of isopropanol with various catalyst and reaction process are presented in **Table 3**.

It can be seen that the zirconium phosphate-supported natural zeolite catalysts provided sufficient catalytic activity toward DIPE production compared to the other reports (Table 3). Based on the previous study [34], the metal phosphate loading during the impregnation process significantly enhanced the dehydration of isopropanol to DIPE, in which high loading of up to 8 mEq/g was found to be sufficient to promote the optimum selectivity and yield towards DIPE. At this condition, the metal-phosphate interaction produced a harmonious effect, which was suggested due to the existence of both Lewis and Bronsted acidic sites, although the textural and the morphological surface might affect the catalytic activity but were slightly dominant.

The Zeolite-$Zr(H_2PO_4)_4$ catalyst, which revealed the highest catalyst activity towards isopropanol dehydration, was further studied regarding reusability and stability at 150 ˚C for 3 h. The catalyst reusability performance over 4 consecutive runs towards isopropanol dehydration is presented in **Fig. 8**. It was evident that isopropanol conversion, DIPE yield, and DIPE selectivity decreased from 66.7% to 55.21%, from 35.85% to 26.65%, and from 35.85% to 26.65%, respectively after 4 consecutive runs of Zeolite-$Zr(H_2PO_4)_4$. The decrease in catalytic activity towards isopropanol conversion was thought to be caused by the leaching of the catalyst's active site during the regeneration process. **Fig. 8** suggested that Zeolite-$Zr(H_2PO_4)_4$ was still relatively stable and active after 4-times reused.

Table 3. Comparison of the previous study on isopropanol dehydration with various catalyst and reaction processes

Catalyst	Reaction process	DIPE selectivity	DIPE yield	IPA conversion	Refs.
SiO_2-ZrO_2 (20-30 mol %)	T= 180-210 ˚C	5-13%	-	10-50%	[11]
γ-Al_2O_3	T= 226.85 ˚C	12%	-	-	[84]
Fe_3O_4/γ-Al_2O_3	P= 0.1 MPa, T= 250 ˚C	55%	-	63%	[13]
ZrO_2	P= 0.1 MPa, T=250 ˚C	45%	-	4%	[85]
NiP-zeolite (8 (mEq/g)	P=150 ˚C t= 3 h catalyst weight= 0.5 g	33%	40%	81.51%	[34]
ZrP-zeolite (8 mEq/g)	P=150 ˚C t= 3 h catalyst weight= 0.5 g	47.8%	35.81%	66.73%	This study

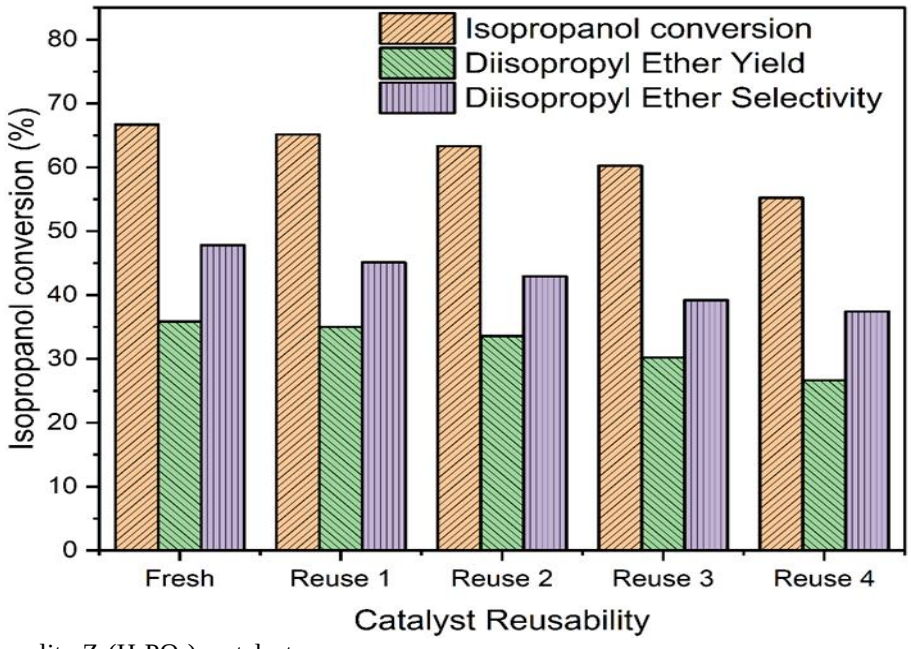

Fig. 8 Reusability of zeolite-$Zr(H_2PO_4)_4$ catalyst

4. Conclusions

The natural zeolite was modified with zirconium and zirconium phosphate and evaluated for the catalytic dehydration of isopropanol to diisopropyl ether (DIPE). The effect of zeolite-Zr$(H_2PO_4)_4$ metal loading on isopropanol dehydration was also assessed. The study revealed that the zeolite was successfully fabricated using zirconium and zirconium phosphate, as corroborated by XRD, FTIR, SEM-EDX, and N_2 physisorption. The isopropanol dehydration revealed that the catalytic activity of zeolite-Zr$(H_2PO_4)_4$ was higher than zeolite-Zr due to high catalyst acidity. The zeolite-Zr$(H_2PO_4)_4$ catalyst with metal loading of 8 mEq/g exhibited the highest catalytic activity towards isopropanol with 66.73% isopropanol conversion, 35.81% DIPE yield, and 47.8% DIPE selectivity. This catalyst had good reusability up to 4 times reused with a slight decrease toward isopropanol conversion due to the catalyst's active site leaching.

Acknowledgements

The authors thank the National Research and Innovation Agency (Badan Riset dan Inovasi Nasional) for instrumental analysis access. We recognize the Biofuel research group, Faculty of Mathematics and Natural Science, Universitas Sriwijaya, for the kind cooperative conduct of the experiment and fruitful discourse.

References

[1] E.P. Sari, K. Wijaya, W. Trisunaryanti, A. Syoufian, H. Hasanudin, W.D. Saputri, Int. J. Energy Environ. Eng. 13 (2022) 967-978.

[2] A.P.F. dos Santos, K.K. da Silva, J. Dweck, L.A. d'Avila, Thermochim. Acta 681 (2019) 178400.

[3] V. Chidambaram B. Viswanathan, Appl. Catal. B Environ. 71 (2007) 32–43.

[4] N. Muñoz-Rujas, J.P. Bazile, F. Aguilar, G. Galliero, E. Montero, J.L. Daridon, Fluid Phase Equilib. 449 (2017) 148-155.

[5] X. Fan, W. Sun, Z. Liu, Y. Gao, J. Yang, B. Yang, C.K. Law, Proc. Combust. Inst. 38 (2021) 321-328.

[6] A.V. Kale A. Krishnasamy, Fuel 314 (2022) 122856.

[7] A. Uyumaz, B. Aydoğan, A. Calam, F. Aksoy, E. Yılmaz, Fuel 265 (2020) 116919.

[8] W. Turek A. Krowiak, Appl. Catal. A Gen. 417–418 (2012) 102-110.

[9] J.E. Rekoske, M.A. Barteau, J. Catal. 165 (1997) 57-72.

[10] J. Escobar, J.A. De Los Reyes, T. Viveros, M. Valle-Orta, M.C. Barrera, Fuel 149 (2015) 109-117.

[11] H.K. Min, Y.W. Kim, C. Kim, I.A.M. Ibrahim, J.W. Han, Y.W. Suh, K.D. Jung, M.B. Park, C.H. Shin, Chem. Eng. J. 428 (2022) 131766.

[12] C.A. Cooper, R.L. McCullough, B.C. Gates, J.C. Seferis, J. Catal. 63 (1980) 372-382.

[13] M.A. Armenta, R. Valdez, R. Silva-Rodrigo, A. Olivas, Fuel 236 (2019) 934-941.

[14] E. López-Salinas, J.G. Hernández-Cortéz, J. Navarrete, M. Salmón, I. Schifter, Stud. Surf. Sci. Catal. 130 (2000) 2591-2596.

[15] C.M. Gómez-Gutiérrez, P.A. Luque, G. Guerra-Rivas, J.A. López-Sánchez, M.A. Armenta, J.M. Quintana, A. Olivas, Scanning 37 (2015) 165-171.

[16] F.P. Heese, M.E. Dry, K.P. Möller, Stud. Surf. Sci. Catal. 130 (2000) 2597-2602.

[17] D.T. Sarve, S.K. Singh, J.D. Ekhe, Inorg. Chem. Commun. 139 (2022) 109397.

[18] E. Ameri, A. Moheb, and S. Roodpeyma, Korean J. Chem. Eng. 28 (2011) 1593.

[19] H. Hasanudin, Q.U. Putri, T.E. Agustina, F. Hadiah, Pertanika J. Sci. Technol. 30 (2022) 377-395.

[20] H. Hasanudin, W.R. Asri, K. Tampubolon, F. Riyant, W. Purwaningrum, and K. Wijaya, Pertanika J. Sci. Technol. 30 (2022) 1739.

[21] H. Hasanudin, W.R. Asri, A. Meilani, N. Yuliasari, Mater. Sci. Forum 1061 (2022) 113-118.

[22] T.K. Phung G. Busca, Chem. Eng. J. 272 (2015) 92-101.

[23] K.A. Tarach, A. Śrębowata, E. Kowalewski, K. Gołąbek, A. Kostuch, K. Kruczała, V. Girman, K. Góra-Marek, Appl. Catal. A Gen. 568 (2018) 64-75.

[24] T. Fujimura, Y.H. Aoyama, R. Sasai, Tetrahedron Lett. 60, (2019) 150912.

[25] D. Li, H. Gong, L. Lin, W. Ma, Q. Zhou, K. Kong, R. Huang, Z. Hou, Mol. Catal. 474 (2019) 110404.

[26] H. Ueoka, O. Shimomura, M. Pica, A. Donnadio, R. Nomura, Colloids Interface Sci. Commun. 28 (2019) 29-33.

[27] F. Xu, H. Zhang, J. Wu, Constr. Build. Mater. 290 (2021) 123208.

[28] R. Bhatt, V. Ageetha, S.B. Rathod, P. Padmaja, Carbohydr. Polym. 208 (2019) 441-450.

[29] H. Hasanudin, W.R. Asri, Q.U. Putri, Z. Fanani, T.E. Agustina, and K. Wijaya, Iran. J. Catal. 12 (2022) 389.

[30] H. Gong, X. Zhao, Y. Qin, W. Xu, X. Wei, Q. Peng, Y. Ma, S. Dai, P. An, Z. Hou, J. Catal. 408 (2022) 245-260.

[31] S. Yu, J. Yan, W. Lin, J. Zhang, J. Long, Catal. Commun. 148 (2021) 106171.

[32] Z. Ye, L. Chen, H. Chen, L. Han, Q. Chen, D. Wang, Chem. Phys. Lett. 709 (2018) 96-102.

[33] Y.A.B. Neolaka, Y. Lawa, J. Naat, A.A.P. Riwu, A.W. Mango, H. Darmokoesoemo, B.A. Widyaningrum, M. Iqbal, H.S. Kusuma, J. Mater. Res. Technol. 18 (2022) 2896–2909.

[34] H. Hasanudin, W.R. Asri, L. Andini, F. Riyanti, A. Mara, F. Hadiah, and Z. Fanani, ACS Omega 7 (2022) 38923.

[35] W. Trisunaryanti, K. Wijaya, T. Triyono, A.R. Adriani, and S. Larasati, Results Eng. 11 (2021) 100258.

[36] G. Kaplan, U. Coskan, A. Benli, O.Y. Bayraktar, A.B. Kucukbaltacı, Constr. Build. Mater. 311 (2021) 125336.

[37] C. Kandilli, Y. Acikbas, M. Uzel, J. Clean. Prod. 318 (2021) 128558.

[38] C. Florez, O. Restrepo-Baena, J.I. Tobon, Constr. Build. Mater. 310 (2021) 125220.

[39] C. Wang, H. Guo, J. Yu, K. Feng, J. Huang, Microporous Mesoporous Mater. 327 (2021) 111430.

[40] Y.A.B. Neolaka, H. Darmokoesoemo, A.A. Adu, Y. Lawa, J. Naat, A.A.P. Riwu, M.F. Bui, E.C. Wila, M.A. Fahirah, T.A. Budiastant, B.A. Widyaningrum, M. Riwu, H.S. Kusuma, J. Mol. Liq. 352 (2022) 118734.

[41] N.J. Abreu, H. Valdés, C.A. Zaror, F. Azzolina-Jury, M.F. Meléndrez, Microporous Mesoporous Mater. 274 (2019) 138-148.

[42] J. Lee, S. Hwang, S.B. Lee, I.K. Song, Korean J. Chem. Eng. 27 (2010) 1755-1759.

[43] H. Ma, J. Zhang, M. Wang, S. Sun, ChemistrySelect 4 (2019) 7981-7990.

[44] N. Mortazavi, M. Bahadori, A. Mari, S. Tangestaninejad, M. Moghadam, V. Mirkhani, I. Mohammadpoor-Baltork, Sustain. Chem. Pharm. 22 (2021) 100495.

[45] E.M. Olegario, C. Mark Pelicano, H.S. Cosiñero, L.V. Sayson, N. Chanlek, H. Nakajima, G.N. Santos, Mater. Lett. 294 (2021) 129799.

[46] H. Valdés, A.L. Riquelme, V.A. Solar, F. Azzolina-Jury, F. Thibault-Starzyk, Sep. Purif. Technol. 258, (2021) 118080.

[47] M.S. Islam, B.J. Mohr, D. VenBerge, J. Build. Eng. 53 (2022) 104535.

[48] B. Mehdi, H. Belkacemi, D. Brahmi-Ingrachen, L.A. Braham, L. Muhr, Groundw. Sustain. Dev. 17 (2022) 100757.

[49] N. Mansouri, N. Rikhtegar, H. Ahmad Panahi, F. Atabi, B.K. Shahraki, Environ. Prot. Eng. 39 (2013) 139-152.

[50] J. Domenzain-Gonzalez, J.J. Castro-Arellano, L.A. Galicia-Luna, M. Rodriguez-Cruz, R.T. Hernez-Lopez, L. Lartundo-Rojas, J. Environ. Chem. Eng. 9 (2021) 105281.

[51] E. Wibowo, M. Rokhmat, Sutisna, R. Murniati, Khairurrijal, M. Abdullah, Mater. Res. Express 4 (2017) 064002.

[52] Y. Zhan, H. Zhang, J. Lin, Z. Zhang, J. Gao, J. Mol. Liq. 243 (2017) 624-637.

[53] M.L. Permata, W. Trisunaryanti, I.I. Falah, M.T. Hapsari, D.A. Fatmawati, Rasayan J. Chem. 13 (2020) 772-779.

[54] L. Wei, N. Kumar, W. Haije, J. Peltonen, M. Peurla, H. Grénman, W. de Jong, Mol. Catal. 494 (2020) 111115.

[55] L. Wei, W. Haije, N. Kumar, J. Peltonen, M. Peurla, H. Grenman, W. de Jong, Catal. Today 362 (2021) 35-46.

[56] L. Alalga, A. Benamar, M. Trari, Int. J. Hydrogen Energy 46 (2021) 28501-28512.

[57] S. Upasen, G. Sarunchot, N. Srira-ngam, Y. Poo-arporn, P. Wattanachai, P. Praserthdam, P. Ngaotrakanwiwat, J. Panpranot, S. Soisuwan, J. CO_2 Util. 55 (2022) 101803.

[58] W. Huang, Q. Wei, Y. Zhou, X. Liu, M. Liu, P. Zhang, Z. Xu, Z. Yu, X. Wang, H. Liu, Catal. Today (2022).

[59] M. Subsadsana, P. Sangdara, C. Ruangviriyachai, Asia-Pacific J. Chem. Eng. 12 (2017) 147-158.

[60] M. Subsadsana C. Ruangviriyachai, Orient. J. Chem. 32 (2016) 839-844.

[61] Sriatun, H. Susanto, Widayat, A. Darmawan, IOP Conf. Ser. Mater. Sci. Eng. 509 (2019) 012138.

[62] Q. Liu, J. Li, Z. Zhao, M. Gao, L. Kong, J. Liu, Y. Wei, J. Catal. 344 (2016) 38-52.

[63] Z. Jiao, Y. Meng, C. He, X. Yin, X. Wang, Y. Wei, Microporous Mesoporous Mater. 318 (2021) 111016.

[64] Y. Gao, M. Li, Y. Ru, J. Fu, Groundw. Sustain. Dev. 13 (2021) 100567.

[65] C. Wang, J. Yu, K. Feng, H. Guo, L. Wang, J. Phys. Chem. Solids 168 (2022) 110827.

[66] H.A.T. Banu, P. Karthikeyan, S. Meenakshi, Results in Surfaces Interfaces 3, (2021) 100010.

[67] S. Kojima, S. Lee, F. Nagata, S. Kugimiya, K. Kato, Mater. Today Commun. 25 (2020) 101310.

[68] A. Ivanets, I. Shashkova, N. Kitikova, A. Radkevich, E. Venhlinskaya, A. Dzikaya, A. V. Trukhanov, M. Sillanpää, Sep. Purif. Technol. 272 (2021) 118912.

[69] P. Zong, M. Shao, X. Xu, M. Xu, N. Yan, S. Wang, Y. Yang, J. Chen, Z. Qiu, J. Mol. Liq. 360 (2022) 119565.

[70] Y. Zhao, S. Yan, Y. He, Z. Li, C. Li, H. Li, Colloids Surfaces A Physicochem. Eng. Asp. 635, (2022) 128084.

[71] J. Wang, Y. Wei, J. Wang, X. Zhang, Y. Wang, N. Li, Ceram. Int. 48 (2022) 12772-12778.

[72] L. Hauli, K. Wijaya, A. Syoufian, Orient. J. Chem. 35 (2019) 128-133.

[73] M.C. Alvarez-Galvan, J.M. Campos-Martin, J.L.G. Fierro, Catalysts 9 (2019) 293.

[74] W. Ni, D. Li, X. Zhao, W. Ma, K. Kong, Q. Gu, M. Chen, Z. Hou, Catal. Today 319 (2019) 66-75.

[75] J. Palomo, J. Rodríguez-Mirasol, T. Cordero, Materials 12 (2019) 2204.

[76] H. Hasanudin, W.R. Asri, M. Said, P.T. Hidayati, W. Purwaningrum, N. Novia, K. Wijaya, RSC Adv. 12 (2022) 16431–16443.

[77] H. Hasanudin, W.R. Asri, I.S. Zulaikha, C. Ayu, A. Rachmat, F. Riyanti, F. Hadiah, R. Zainul, R. Maryana, RSC Adv. 12 (2022) 21916–21925.

[78] M.D. Argyle, C.H. Bartholomew, Catalysts 5 (2015) 145-269.

[79] F. Yaripour, M. Mollavali, S.M. Jam, H. Atashi, Energy Fuels 23 (2009) 1896-1900.

[80] A.E.A.A. Said M.A. El-Aal, J. Fuel Chem. Technol. 46 (2018) 67-74.

[81] W. Ni, D. Li, X. Zhao, W. Ma, K. Kong, Q. Gu, M. Chen, Z. Hou, Catal. Today 319 (2019) 66-75.

[82] S. Li, M. Wen, H. Chen, Z. Ni, J. Xu, J. Shen, J. Catal. 350 (2017) 141-148.

[83] A.A. Rownaghi, F. Rezaei, M. Stante, J. Hedlund, Appl. Catal. B Environ. 119–120 (2012) 56-61.

[84] W. Turek, J. Haber, and A. Krowiak, Appl. Surf. Sci. 252 (2005) 823.

[85] J.G. Hernández-Cortez, E. López-Salinas, M. Manríquez, M. Picquart, Mater. Res. Soc. Symp. Proc. 1279 (2010) 109-121.